Supporting Informatin

A stable anionic metal-organic framework with open coordinated sites: selective separation toward cationic dyes and sensing properties

Wei Gao[ab], Feng Liu[b], Chang-Wei Pan[a], Xiu-Mei Zhang[*bc], Jie-Ping Liu[b] and Qing-Yu Gao[*a]

Table S1 Crystal data and structure refinement for Cd-MOF-**1**

	Cd-MOF-**1**
Empirical formula	$C_{48}H_{38}Cd_3N_6O_{17}$
Formula weight	1308.07
Crystal system	Monoclinic
Space group	$P2_1/c$
a /Å	17.960(4)
b /Å	12.903(2)
c /Å	24.414(4)
α /°	90
β /°	127.047(11)
γ /°	90
V /Å^3	4515.6(14)
Z	4
D_c (g m^{-3})	1.924
μ (mm^{-1})	1.487
F(000)	2592
Reflections collected	24028
Unique reflections	7740
GOF on F^2	1.012
R_{int}	0.0780
*R*1 [$I>2\sigma(I)$]	0.0453
*wR*2 (all data)	0.1056

Table S2 Selected bond lengths (Å) and angles (°) for Cd-MOF-**1**.

Cd-MOF-**1**			
Cd1-O1	2.342(4)	Cd1-O2	2.369(4)
Cd1-O4A	2.263(4)	Cd1-O7	2.441(5)

Cd1-O8	2.323(4)	Cd1-O14	2.194(4)
Cd2-O14	2.229(4)	Cd2-O10B	2.270(5)
Cd2-O5C	2.305(5)	Cd2-O15	2.333(5)
Cd2-N4D	2.351(5)	Cd2-O3A	2.405(5)
Cd3-O14	2.227(4)	Cd3-O9B	2.278(5)
Cd3-O12E	2.290(5)	Cd3-O13	2.322(5)
Cd3-O6C	2.335(5)	Cd3-N3	2.344(5)
O14-Cd1-O4A	93.01(16)	O14-Cd1-O8	104.22(16)
O4A-Cd1-O8	91.39(17)	O14-Cd1-O1	102.38(16)
O4A-Cd1-O1	119.47(17)	O8-Cd1-O1	137.66(17)
O14-Cd1-O2	153.21(15)	O4A-Cd1-O2	86.61(17)
O8-Cd1-O2	102.58(16)	O1-Cd1-O2	55.79(16)
O14-Cd1-O7	99.80(17)	O4A-Cd1-O7	146.10(17)
O8-Cd1-O7	55.11(17)	O1-Cd1-O7	88.35(16)
O2-Cd1-O7	95.19(18)	O14-Cd2-O10B	108.10(16)
O14-Cd2-O5C	91.49(16)	O10B-Cd2-O5C	91.49(16)
O14-Cd2-O15	83.39(16)	O10B-Cd2-O15	166.85(17)
O5C-Cd2-O15	95.96(17)	O14-Cd2-N4D	168.19(17)
O10B-Cd2-N4D	83.24(18)	O5C-Cd2-N4D	91.76(18)
O15-Cd2-N4D	84.98(18)	O14-Cd2-O3A	81.23(15)
O10B-Cd2-O3A	86.87(17)	O5C-Cd2-O3A	170.91(16)
O15-Cd2-O3A	88.65(16)	N4D-Cd2-O3A	96.46(18)
O14-Cd3-O9B	92.65(17)	O14-Cd3-O12E	86.89(16)
O9B-Cd3-O12E	170.98(17)	O14-Cd3-O13	90.46(16)
O9B-Cd3-O13	84.94(19)	O12E-Cd3-O13	104.07(19)
O14-Cd3-O6C	99.42(16)	O9B-Cd3-O6C	99.42(16)
O12E-Cd3-O6C	85.36(18)	O13-Cd3-O6C	166.77(18)
O14-Cd3-N3	169.03(18)	O9B-Cd3-N3	96.6(2)
O12E-Cd3-N3	84.85(19)	O13-Cd3-N3	84.57(19)

O6C-Cd3-N3	87.11(18)

Symmetry codes: A -x+1, y+1/2, -z+3/2; B -x+2, -y+1, -z+2; C -x+1, -y+1, -z+1; D x-1, -y+3/2, z-1/2; E -x+2, y+1/2, -z+3/2.

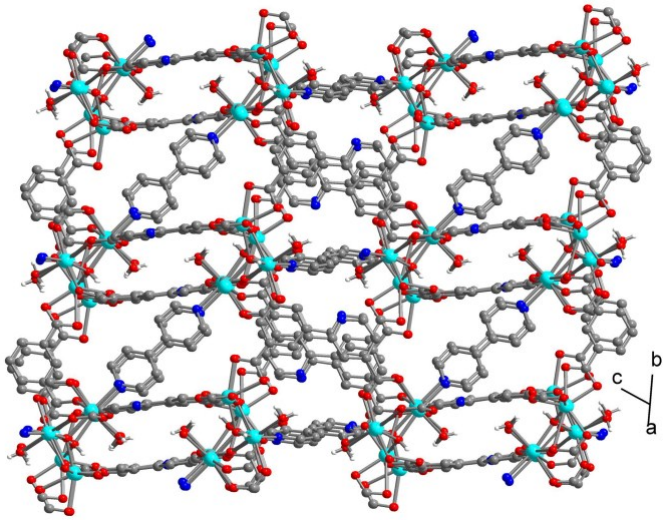

Fig. S1 3D framework with accessible Lewis-base sites of Cd-MOF-**1**.

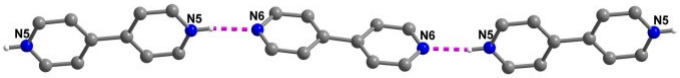

Fig. S2 The hydrogen-bonded chains of Cd-MOF-**1**.

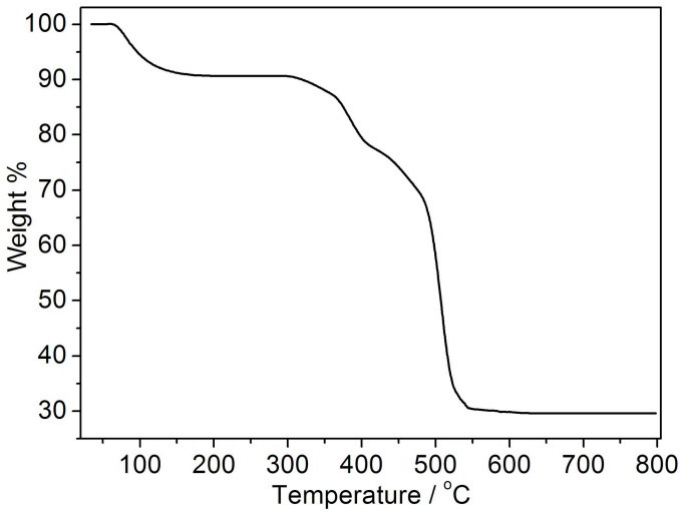

Fig. S3 TGA curve of Cd-MOF-**1**.

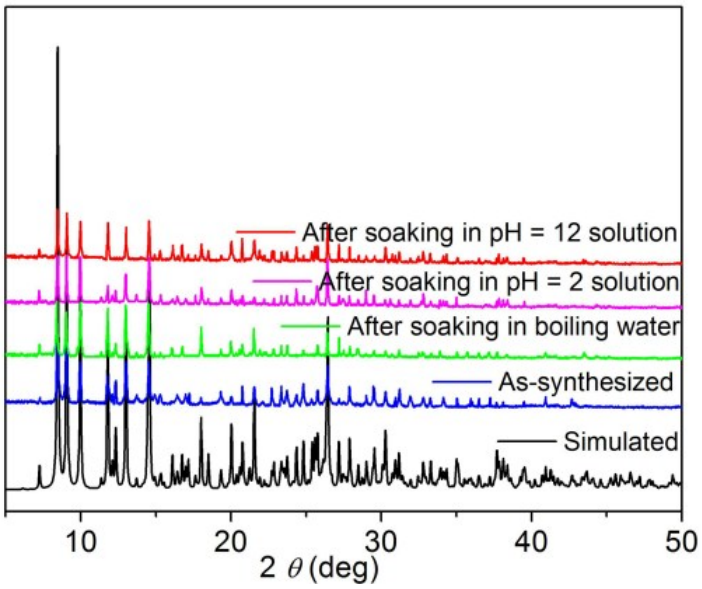

Fig. S4 PXRD patterns of Cd-MOF-**1** in different pH values in the range of 2-12 and the boiling water.

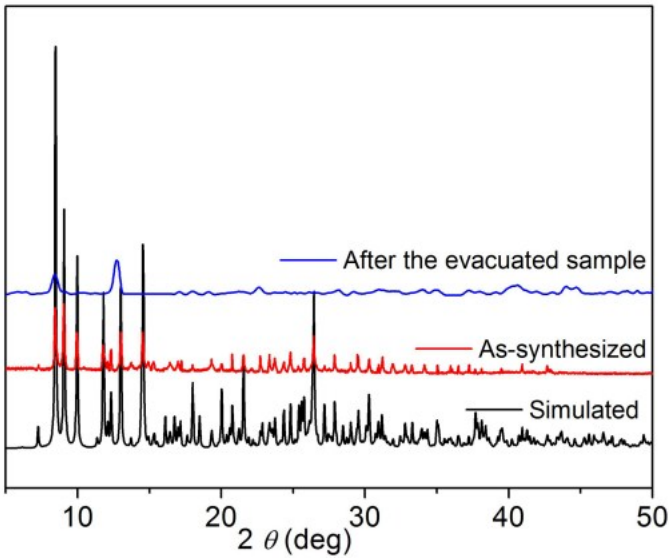

Fig. S5 PXRD patterns of Cd-MOF-**1**: (black line) simulated from the single-crystal data, (red line) for the as-synthesized sample, (blue line) for the evacuated sample.

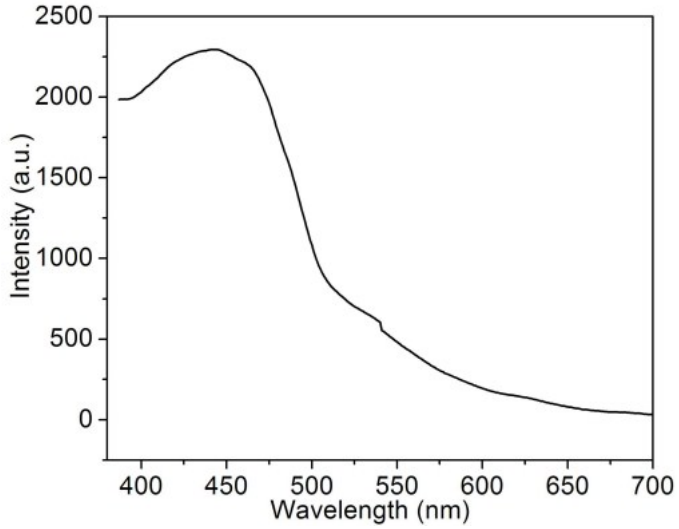

Fig. S6 Solid state emission spectra (λ_{ex} = 357 nm) of free H_3L ligand at room temperature.

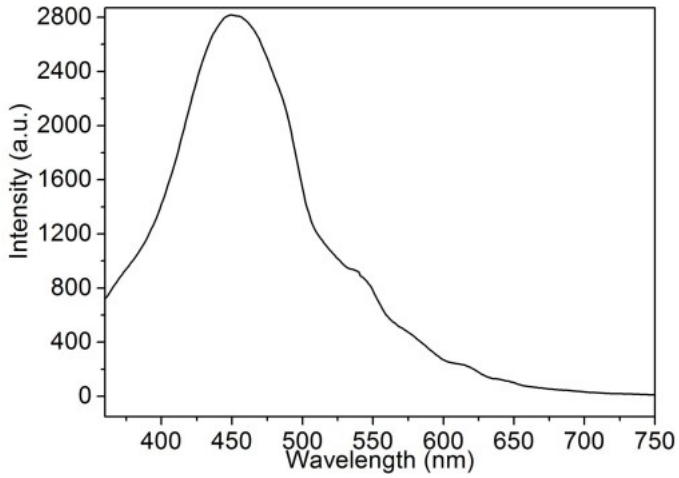

Fig. S7 Solid state emission spectra of Cd-MOF-**1**.

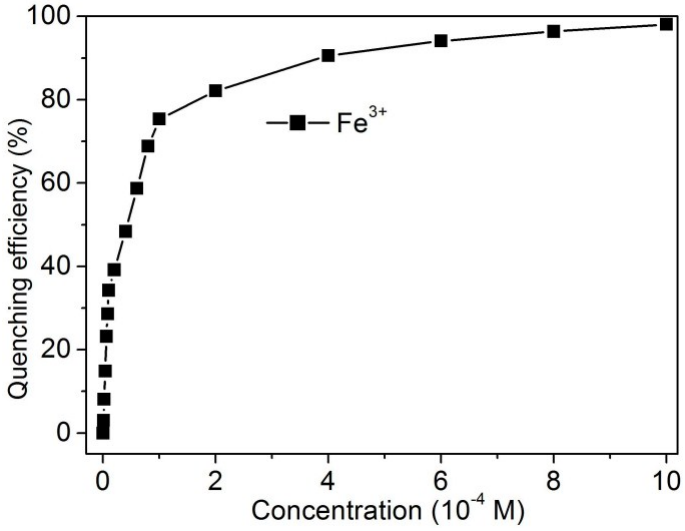

Fig. S8 Dependence of the quenching efficiency on the concentration of Fe^{3+} ions.

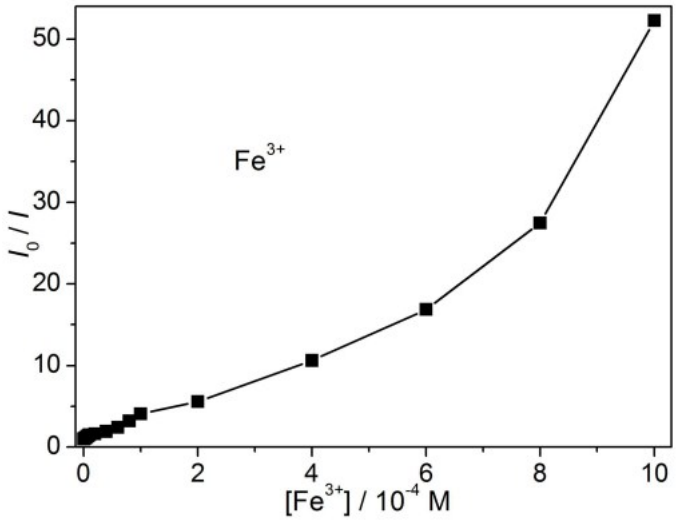

Fig. S9 The Stern-Volmer plot of I_0/I *vs* Fe^{3+} concentration for Cd-MOF-**1**.

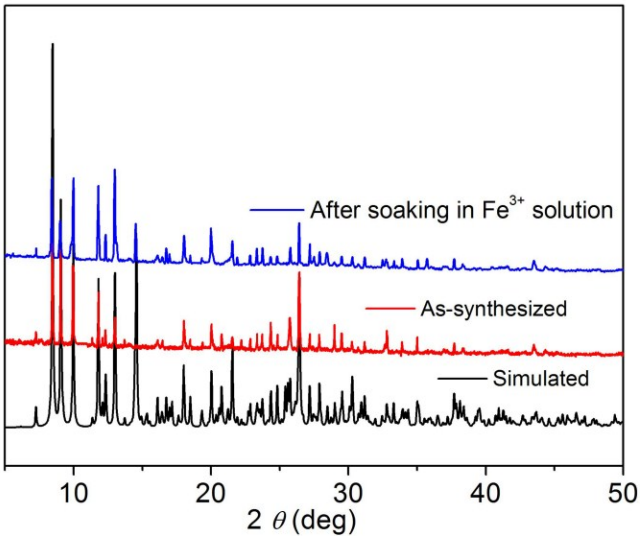

Fig. S10 The powder X-ray diffraction patterns of simulated Cd-MOF-**1**, as-synthesized Cd-MOF-**1** and Cd-MOF-**1** immersed in 1.0 mM water solutions of Fe^{3+} ions.

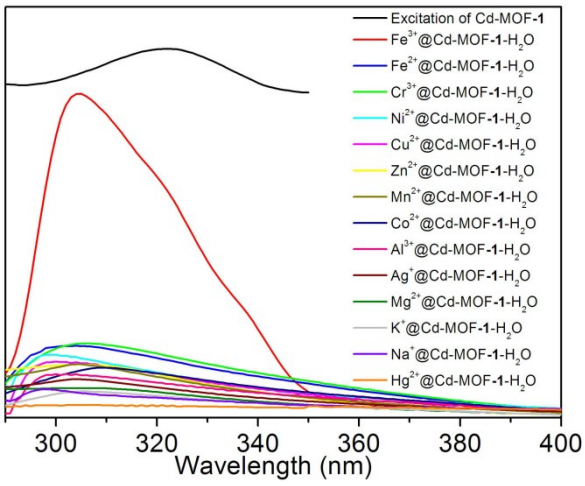

Fig. S11 The UV-Vis absorption spectra of Cd-MOF-**1** immersed in different metal ions and the excitation for Cd-MOF-**1**.

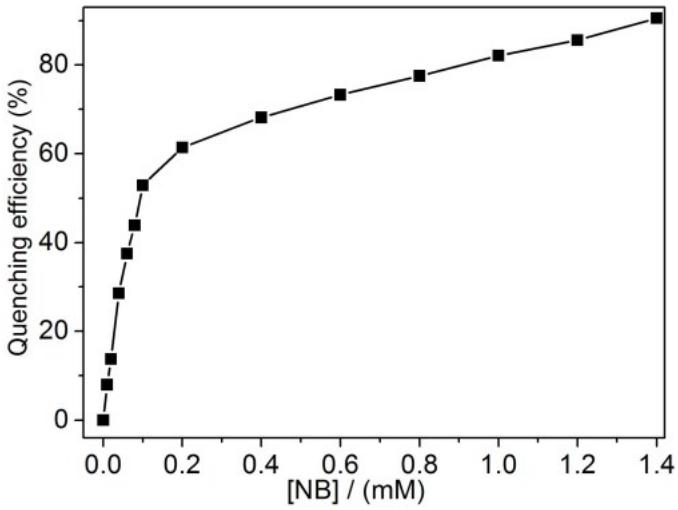

Fig. S12 Dependence of the quenching efficiency on the concentration of NB.

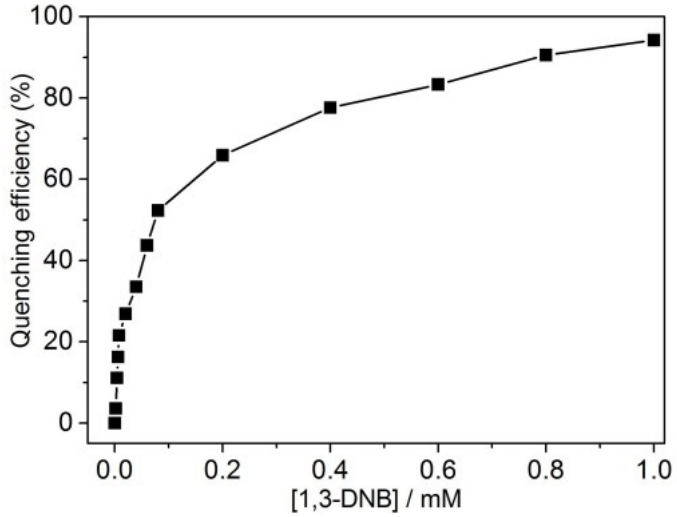

Fig. S13 Dependence of the quenching efficiency on the concentration of 1,3-DNB.

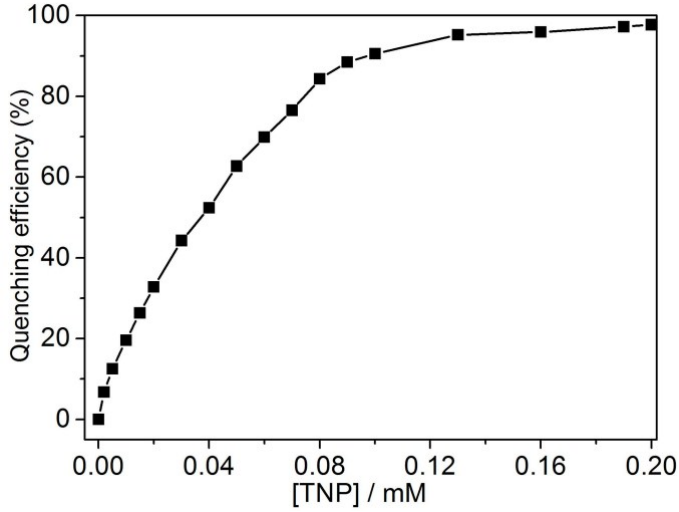

Fig. S14 Dependence of the quenching efficiency on the concentration of TNP.

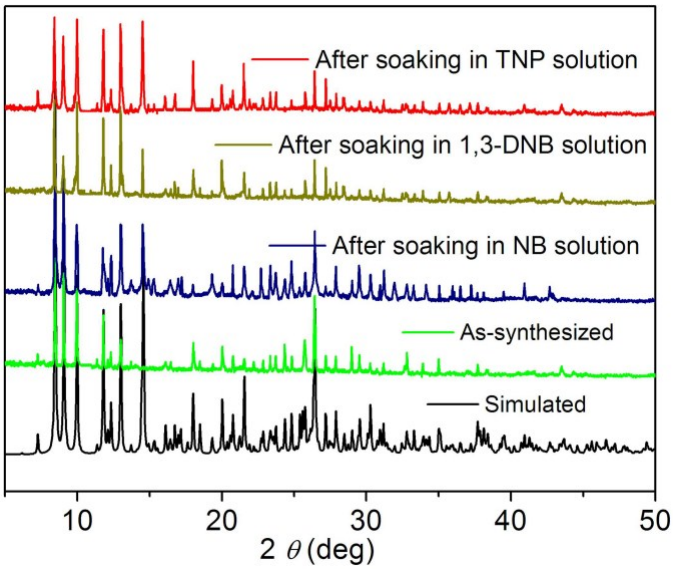

Fig. S15 The powder X-ray diffraction patterns of simulated Cd-MOF-**1**, as-synthesized Cd-MOF-**1** and Cd-MOF-**1** immersed in 1.0 mM EtOH solutions of NB, 1,3-DNB and TNP.

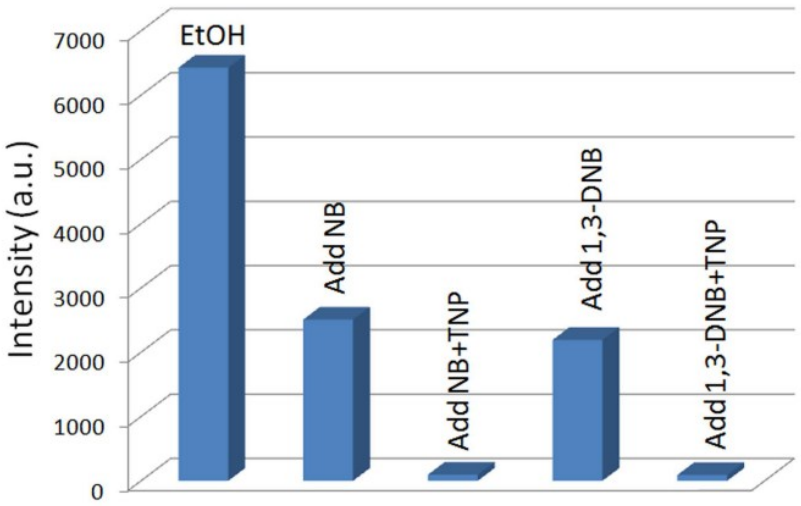

Fig. S16 The luminescence intensity at 454 nm of Cd-MOF-**1** soaking in the single and mixed NACs EtOH solutions with TNP.

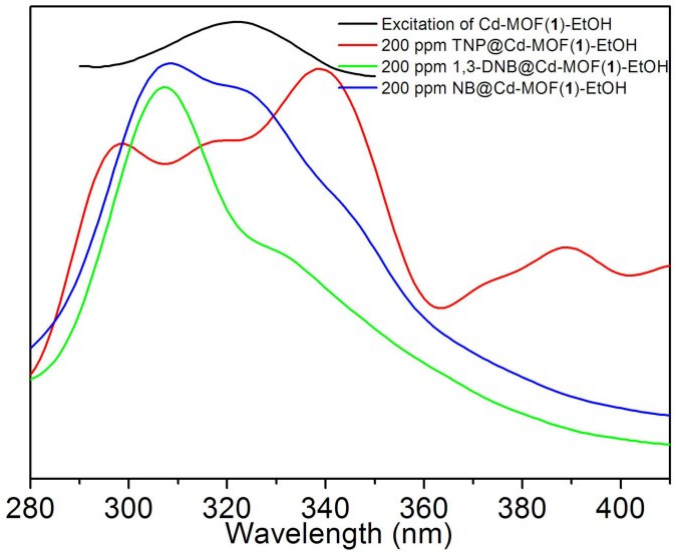

Fig. S17 The UV-Vis absorption spectrum of EtOH solutions of different testing nitro explosives (NB, 1,3-DNB and TNP) and the excitation for Cd- MOF-**1**.

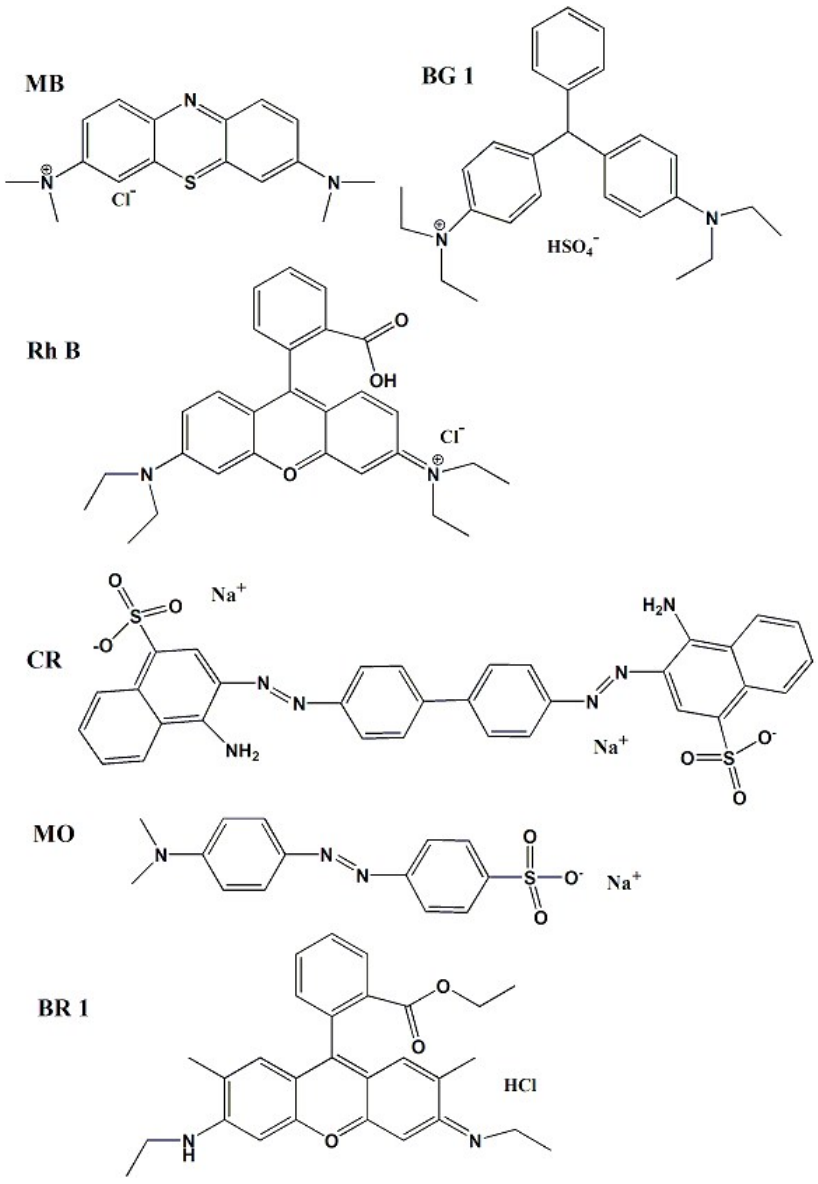

Fig. S18 The structures of dye molecules that were used in the dye adsorption and separation experiment.

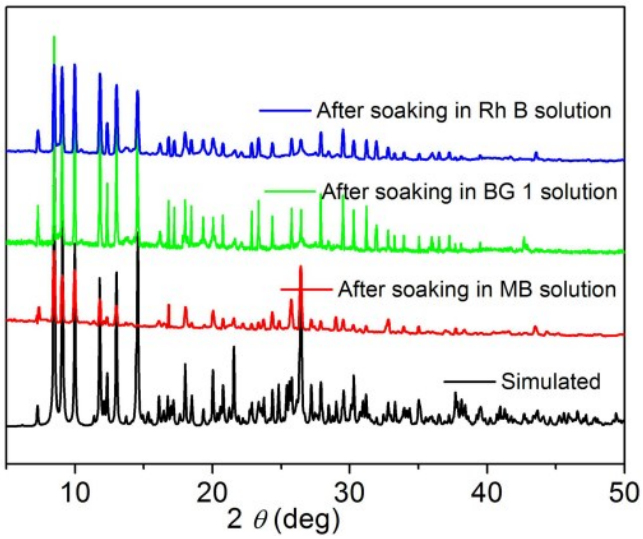

Fig. S19 XRPD patterns of simulated Cd-MOF-**1** (black), and after the absorption of MB (red), BG 1 (green) and Rh B (blue), respectively.

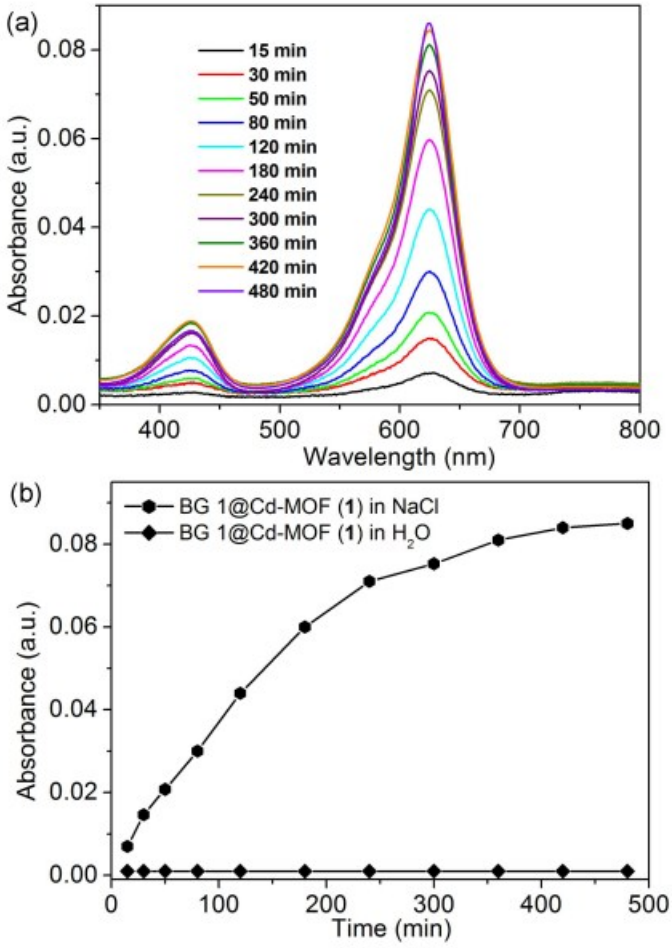

Fig. S20 (a) UV-vis spectra of the BG1 released from BG 1@Cd-MOF-**1** in a saturated NaCl aqueous solution; (b) The release-rate comparison of BG 1 from BG 1@Cd-MOF-**1** in a saturated NaCl aqueous solution and deionized water.

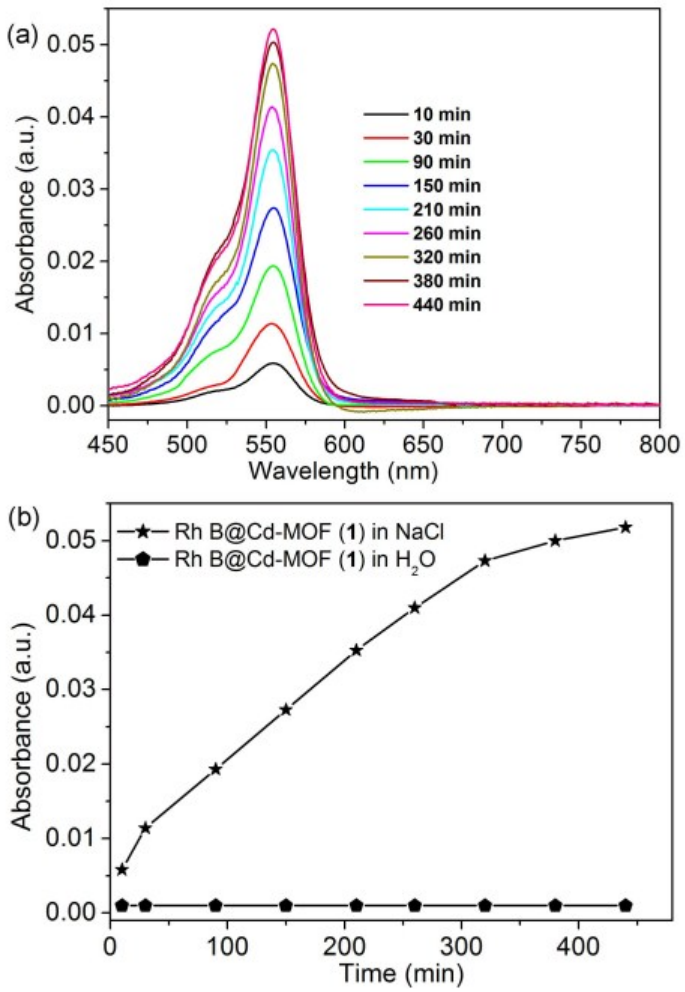

Fig. S21 (a) UV-vis spectra of the Rh B released from Rh B@Cd-MOF-**1** in a saturated NaCl aqueous solution; (b) The release-rate comparison of Rh B from Rh B@Cd-MOF-**1** in a saturated NaCl aqueous solution and deionized water.